Thermal Analysis of the Formation of Chunky Graphite during Solidification of Heavy-section Spheroidal Graphite Iron Parts

Jon Sertucha, Ramon Suarez, Iker Asenjo, Peio Larrañaga, Jacques Lacaze, Inaki Ferrer, Susana Armendariz

ISIJ International, Vol. 49 (2009), No. 2, pp. 220–228

Thermal Analysis of the Formation of Chunky Graphite during Solidification of Heavy-section Spheroidal Graphite Iron Parts

Jon SERTUCHA,[1)] Ramón SUÁREZ,[1)] Iker ASENJO,[1)] Peio LARRAÑAGA,[1)] Jacques LACAZE,[2)] Iñaki FERRER[3)] and Susana ARMENDARIZ[3)]

1) Engineering and Foundry Department, AZTERLAN, Aliendalde auzunea 6, E-48200 Durango (Bizkaia), Spain.
2) Université de Toulouse, CIRIMAT, UMR 5085, 31077 Toulouse cedex 4, France.
3) TS Fundiciones, S.A. Pol. Sansinenea Erreka, E-20749 Arroa-Zestoa (Gipuzkoa), Spain.

(*Received on September 12, 2008; accepted on November 6, 2008*)

Analysis of cooling curves recorded at the centre of large blocks cast with near-eutectic spheroidal graphite cast irons prone to give chunky graphite has been checked against microstructure observations. It has been observed that solidification proceeds totally at temperatures lower than the stable eutectic temperature and the following solidification sequence could be proposed: 1) nucleation of primary graphite in the liquid; 2) initial eutectic reaction processing by growth of austenite-like dendrites encapsulating the primary nodules; 3) bulk eutectic reaction related to nucleation and then growth of CHG cells and of secondary nodules, these latter giving spheroidal graphite eutectic cells. It was found that the maximum recalescence during the eutectic reaction first increases with the volume of the block affected by chunky graphite, and then decreases when most of the material is affected. Interestingly enough, a relationship between the volume of the blocks affected by CHG and the recalescence measured on TA cups has been observed.

KEY WORDS: heavy-section castings; spheroidal cast iron; graphite degeneracy; chunky graphite; thermal analysis.

1. Introduction

Thermal analysis (TA) has been used since long for characterizing melt preparation of cast irons, most often for checking composition before pouring but more and more as a means for providing information on the main phase transformations occurring upon cooling from the liquid state. Owing to the relationship between cooling curves characteristics and microstructure features, thermal analysis has thus been developed for obtaining information regarding graphite morphology[1–6)] as well as nucleation potential of graphite during solidification and inoculation efficiency.[7–10)] It has been further extended for latent heat evaluation[4,11–13)] and for improving process variables,[7–8,14–18)] *e.g.* with the aim at predicting final mechanical properties and hardness values[19,20)] or for minimizing casting defects such as shrinkage tendency.[6,21,22)]

Thermal analysis, in particular carried out with standard thermal cups, has been successful in relating characteristics of the solidification step as observed on cooling curves with microstructure changes caused by modification of the composition and of the nucleation potential of the melt. Less successful results have been achieved for predicting graphite shape when the microstructure of post-inoculated spheroidal, compacted and lamellar cast irons samples has been compared to the characteristics of the cooling curves.[3–5,8,15)]

This limitation of TA is quite unfortunate when dealing with large melts prepared for thick-wall ductile iron castings. In these cases where cooling rate becomes extremely low and where cooling curves are characterised by lengthy eutectic plateaus,[23–26)] the solidification microstructure may be affected by magnesium and inoculation fading, marked intercellular segregation, as well as graphite degeneracy. Among the various forms of degenerate graphite observed, chunky graphite (hereafter denoted CHG) turns out to be the most critical defect due to its negative influence on mechanical properties.[25,27)] Graphite degeneracy in large section castings has been extensively studied since the 60's and its formation or avoidance has been often related to the presence of low-level elements.[28–35)] Limited amounts of rare earths, lead and antimony added to the melt help avoiding CHG.[31–33,36,37)] Also, the use of chills has been found efficient to suppress CHG formation,[23,24,38,39)] but this is limited to thicknesses up to a few centimetres.

As done for the thermal analysis performed on standard cups, description of the cooling curves recorded during solidification of heavy sections, either or not with chills, has been given since long.[23,24,26,34,40)] Some work was also done recently aimed at relating thermal analysis made on standard cups to characteristics of degenerated graphite microstructure in large castings,[41)] that seems unsuccessful in view of the spreading of the reported data. Because of the lack of success of TA to help understanding CHG formation, various authors made laboratory studies where solidification of limited quantities of metal was controlled so as to reproduce the cooling schedule of large castings with quenching at critical times during the eutectic reaction.[42–45)]

Table 1. Chemical composition of the alloys (wt%). Numbers between brackets in the first row give the accuracy for each element.

Code	C (0.06)	Si (0.02)	P (0.004)	Cu (0.005)	Cr (0.002)	Ni (0.007)	Mn (0.01)	Mg (0.004)	S (0.001)	Sb (0.0002)	Pb (0.0002)	Ce (0.0002)	C_{eq}	T_{eut}
M5-4	3.72	2.35	0.034	0.01	0.02	0.01	0.10	0.036	0.007	<0.0002	<0.0002	0.0022	4.38	1164.0
M5-5	3.61	2.28	0.036	0.01	0.02	0.01	0.20	0.043	0.009	<0.0002	<0.0002	0.0027	4.25	1163.7
M5-6	3.68	2.23	0.039	0.01	0.02	0.01	0.21	0.052	0.013	<0.0002	<0.0002	0.0023	4.30	1163.5
M5-10	3.64	2.19	0.036	0.01	0.02	0.01	0.11	0.041	0.012	<0.0002	<0.0002	0.0025	4.25	1163.3
M5-11	3.72	2.20	0.039	0.02	0.02	0.01	0.10	0.040	0.011	<0.0002	<0.0002	0.0028	4.34	1163.3
M5-12	3.68	2.20	0.035	0.02	0.02	0.01	0.09	0.040	0.014	<0.0002	<0.0002	0.0123	4.30	1163.3
M5-13	3.73	2.08	0.035	0.03	0.02	0.01	0.013	0.052	0.009	<0.0002	<0.0002	0.0162	4.31	1162.8
M5-16	3.72	2.08	0.032	0.01	0.03	0.01	0.15	0.042	0.003	<0.0002	<0.0002	0.0100	4.30	1162.8
M5-18	3.71	2.07	0.034	0.03	0.03	0.01	0.15	0.038	0.006	<0.0002	<0.0002	0.0028	4.29	1162.7

All these studies conclusively showed that solidification proceeds first by the formation of nodular graphite and austenite dendrites, the former being encapsulated within the latter. This is only in a second stage that cells of CHG appear that nucleate at the austenite/liquid interface. Thanks to these laboratory experiments, it appeared of some interest to challenge again the analysis of cooling curves obtained during solidification of thick-wall castings. In the present work, the cooling curves recorded during castings of large blocks and standard TA cups are first described and compared. The possibility of correlating cooling curve characteristics with microstructure information and CHG formation is then discussed. Lines for further investigations are finally drawn from these results.

2. Experimental Details

The experimental study was performed on large cubic blocks cast in sand. All details about the casting methodology have been given in a previous work, including indications on the metallic charges used and the treatments performed for pre-inoculation and spheroidization.[46] In this work, emphasis was put on the effect of post-inoculation in the mould on the extent of the area affected by CHG formation. All the cast blocks were in fact equipped with a K-type thermocouple positioned at the geometrical centre for recording the cooling curves during solidification. While the previous work dealt with cubic blocks 180 and 300 mm in size, it appeared necessary in the present report to select only the larger blocks for clarity. These blocks have a thermal modulus (ratio of their volume to their outer area available for heat-exchange) of 5 cm. In most experiments, couples of blocks of similar modulus were cast at the same time using post-inoculated and non post-inoculated melts. For differentiating the various blocks that were cast, they will be denoted M5-Y-Z where:

- M5 relates to the thermal modulus of the cubes;
- Y is the experiment number (1, 2, 3, …);
- Z is either I or N to indicate post-inoculated (I) or non post-inoculated (N) block.

In order to determine the chemical composition of the melt, a metal sample was taken just before pouring the iron into the moulds that was afterwards analysed by combustion techniques using a Leco CS 244 equipment for determining C and S contents, inductively coupled plasma and mass spectrometry (ICP-MS Agilent 7500ce) for Sb, Pb and Ce, gravimetric procedures for Si and optical emission spectrometry (OBLF QS750) for P, Cu, Cr, Ni, Mn and Mg. The chemical compositions are listed in **Table 1**, where is given also the expected accuracy for each element. Because all alloying elements other than silicon are at very low level, the carbon equivalent of the alloys may be simply written as $C_{eq}=W_C+0.28\times W_{Si}$, where W_i designates the weight percent content of element "i" in the alloy.[47] Also, the corresponding stable eutectic temperature T_{eut} may be evaluated as $T_{eut}=1154.0+4.244\times W_{Si}$ (°C).[47] Values of both C_{eq} and T_{eut} have been added in Table 1. With eutectic composition assumed at $C_{eq}=4.34$ wt%, it is seen that the carbon equivalent C_{eq} varies from a slightly hypoeutectic to a slightly hypereutectic composition (4.25 to 4.38 wt%) while the stable eutectic temperature ranges from 1162.7 to 1164.0°C. Note that the C_{eq} values should normally differ for inoculated and non-inoculated castings from the same melt. For usual inoculation as the one carried out in this work, the related increase in silicon content amounts to about 0.14 wt% Si, that corresponds to an 0.04 wt% increase in the carbon equivalent value.

After cooling, all blocks were cut along vertical axes and the sections examined for determining the amount of CHG according to the methodology described previously[46] in which it was characterized by the two quantities V_V and A_A. The fraction of the volume of the block affected by CHG, denoted V_V, was evaluated by means of macrographic observation. The surface fraction of CHG cells, A_A, at the centre of the blocks was measured on five different optical micrographs. On the same metallographic sections, the nodule count at the centre of the blocks, N_{block}, was evaluated on five different optical micrographs obtained at an enlargement of ×100 in areas where the graphite was correctly formed. For this evaluation, only particles with an area larger than 20 μm^2 were considered, this corresponding to nodules with diameter larger than 5 μm. Please note that the data given previously[46] have been slightly corrected in the present work.

At the time of pouring, two standard TA cups (inoculated and non inoculated) were simultaneously filled and their cooling curves recorded using the Thermolan® system.[22] The additionnal inoculation was performed by adding in the cup a convenient amount of the same inoculant than the one used for post-inoculation of the blocks. This addition was made by powdering a mass of inoculant such as to reach the same inoculation level than for blocks. The cooling curves were subsequently analysed for determining the characteristic solidification temperatures. Also, on one occasion, one

of the blocks was quenched at about one third of the expected solidification time. In that case, the mould-block system was moved into a holder containing water when the temperature record reached the minimum during the eutectic reaction. After the mould was plunged into the water tank, part of the sand was removed so as to increase the chilling effect.

3. Results

Figure 1(a) presents the cooling records obtained with TA cups for inoculated (solid line) and non-inoculated (interrupted line) M5-11 alloy and for inoculated M5-6 one (solid line, shifted along the x axis for clarity). For inoculated alloys, the TA curves show either one or two significant thermal arrests, while there are always two thermal arrests for non inoculated alloys. The cooling curves recorded on the blocks show one, two or three arrests, with increasing length as illustrated in Fig. 1(b) in the case of M5-16-I and M5-16-N castings. These features are much alike those described by Chaudhari *et al.*,[1] namely that solidification proceeds in three successive steps: i) primary deposition of either austenite or graphite; ii) initial and limited growth of eutectic; and iii) bulk eutectic growth. Following the labelling used by these authors, the characteristic temperatures will be denoted T_L and T_{EN} for the first and second arrests, and T_{EU} and T_{ER} for the minimum and maximum bulk eutectic temperatures (see Fig. 1). As a matter of fact, the first reaction (T_L) was hardly observed on the TA cups and did not always show up in the case of the blocks.

As some recalescence may sometimes be observed during the first and second reactions when present, superscripts 1 and 2 will be used to denote the related minimum and maximum temperatures. Accordingly, a cooling curve may be characterized by up to six characteristic temperatures: T^1_L and T^2_L, T^1_{EN} and T^2_{EN}, T_{EU} and T_{ER}. All the characteristic temperatures evaluated from the set of cooling curves recorded on the cast blocks and TA cups are listed in **Table 2**. When either of the first two reactions appears without recalescence, its characteristic temperature is determined at the inflexion point of the thermal arrest and associated to

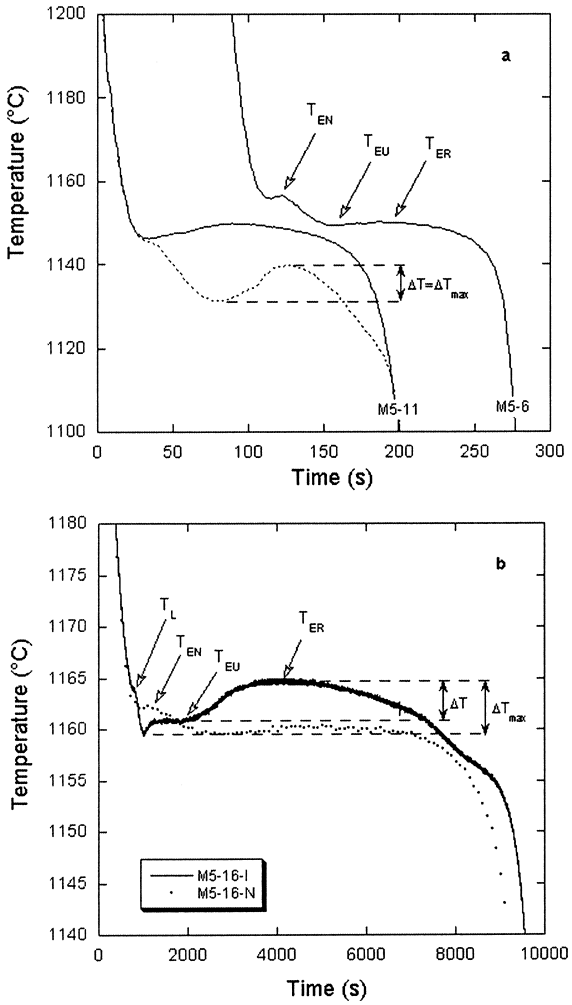

Fig. 1. Example of cooling curves recorded from M5-6 and M5-11 TA-cups (a) and from blocks M5-16-I and M5-16-N (b). Solid (resp. dotted) lines relate to melts with (resp. without) post-inoculation. In Fig. 1(a), the curve for alloy M5-6 has been shifted along the x axis for clarity. The recalescence during the bulk eutectic reaction, ΔT, and the maximum recalescence, ΔT_{max}, have been indicated on the curve for block M5-16-I. These values are sometimes equal for blocks and always for TA cups (see text).

Table 2. Characteristic temperatures (°C) evaluated on TA cups and blocks. I (respectively N) stand for blocks with (respectively without) post-inoculation.

Code	TA cups				Blocks					
	T^1_{EN}	T^2_{EN}	T_{EU}	T_{ER}	T^1_L	T^2_L	T^1_{EN}	T^2_{EN}	T_{EU}	T_{ER}
M5-4-I	---	---	1146.1	1150.3	---	---	1152.6	1157.0	1157.0	1157.9
M5-4-N	---	1146.0	1140.0	1147.2	---	---	1151.5	1153.5	1153.5	1157.5
M5-5-I	---	1161.1	1147.2	1149.3	---	---	1163.0	1164.0	1156.2	*
M5-5-N	---	1160.2	1135.5	1141.4	---	---	1166.1	1167.6	1153.6	1154.8
M5-6-I	1155.8	1156.5	1149.3	1150.2	---	---	1158.8	1160.3	1153.0	1155.3
M5-6-N	---	1156.2	1134.1	1138.0	---	---	1162.8	1164.2	1155.1	1158.0
M5-10-I	---	---	1144.2	1147.7	1156.6	1156.8	---	---	1152.8	1157.9
M5-10-I#	---	---	1144.2	1147.7	---	---	1151.1	1153.0	**	**
M5-10-N	1143.5	1143.5	1140.2	1144.6	---	---	---	---	1150.8	1158.6
M5-11-I	---	---	1146.2	1149.9	---	1158.2	---	---	1152.2	1157.8
M5-11-N	1145.4	1145.4	1131.2	1139.9	---	---	1150.2	1151.7	1151.5	1154.7
M5-12-I	---	---	1145.8	1149.0	---	---	---	---	1151.5	1157.8
M5-13-I	1146.9	1147.7	1145.8	1147.7	1161.5	1161.6	1154.6	1157.8	1157.8	1161.2
M5-13-N	---	1146.9	1135.0	1136.8	1161.1	1161.4	1155.1	1155.7	1155.2	1156.5
M5-16-I	1146.9	1147.7	1144.8	1145.4	---	1163.8	1159.5	1160.7	1160.7	1164.9
M5-16-N	---	1146.9	1138.7	1139.3	1163.1	1163.4	1161.8	1162.5	1159.2	1160.4
M5-18-I	1149.6	1150.2	1147.9	1148.7	---	1162.4	1160.3	1161.1	1159.4	1162.6

* thermocouple broke during solidification

** Block chilled in water.

T_L^2 or T_{EN}^2, while no value is given to T_L^1 or T_{EN}^1. When the first reaction was not observed, no T_L value is reported. Further, the second and third reactions sometimes overlapped as for the inoculated block in Fig. 1(b), in which case the T_{EN}^2 and T_{EU} values are set equal and estimated at the inflexion point between the two thermal arrests. On some occasions these two thermal arrests merged in one single peak and only the T_{EU} and T_{ER} temperatures are then given. In one case, block M5-5-I, the thermocouple broke during solidification so that the maximum eutectic temperature could not be estimated.

For further analysis of the cooling records, recalescence values for the eutectic reaction were estimated from the characteristic temperatures listed in Table 2. In the case of TA cup records, the recalescence ΔT is uniquely defined as $\Delta T=(T_{ER}-T_{EU})$. For records from the blocks, the maximum recalescence $\Delta T_{max}=(T_{ER}-T_{min})$, where T_{min} is the minimum temperature reached during solidification that may be either T_{EN}^1 or T_{EU}, may differ from the recalescence associated to the bulk eutectic reaction, $\Delta T_{EU}=(T_{ER}-T_{EU})$. This is due to the fact that the initial eutectic reaction may proceed at temperature either lower or higher than T_{EU}. This is the case of the curves in Fig. 1(b) and is again illustrated in Fig. 6.

In a first step, the characteristics of the cooling curves obtained from TA cups and blocks were compared. **Figure 2** shows the plot of the maximum eutectic temperature T_{ER} *versus* T_{EU} for both TA cups and blocks. As expected, the temperature range for the eutectic reaction is shifted to higher values when the cooling rate is decreased, from TA cups to blocks. The symbols used in the plot allow differentiating data from post-inoculated and non post-inoculated materials. It is thus interesting to note that the data for the TA cups shows clearly the effect of post-inoculation on the temperature range for the eutectic reaction, while all the points from the blocks are interspersed in the same area of the graph. The difference between the interrupted and solid lines along the y axis represents the scattering band for recalescence values. It is noteworthy that in the case of the TA cup records recalescence appears significantly smaller for post-inoculated melts than for non post-inoculated ones. Also, the relatively large recalescence values observed on blocks are worth of mention as further stressed later. If T_{min} had been employed instead of T_{EU} to report the data from the blocks, the graph would have been similar with however some even higher recalescence values.

The set of T_{ER} values has been plotted again in **Fig. 3** *versus* the corresponding values of T_{EU} measured on TA cups. The points for TA cups are the same than in Fig. 2 while those for blocks are now separated in relation to the use or not of post-inoculation. It is seen that there may be a slight positive correlation between the T_{ER} values measured on non post-inoculated blocks and the T_{EU} values measured on the corresponding TA cups. Though the data is quite scattered, the correlation seems inverted in the case of post-inoculated blocks. Alongside the points related to the blocks, the nodule counts measured on blocks, N_{block}, that are listed in **Table 3** have been reported. While there is a clear difference between the average values for non post-inoculated and post-inoculated blocks, it is worth stressing that no correlation could be evidenced between T_{ER} values

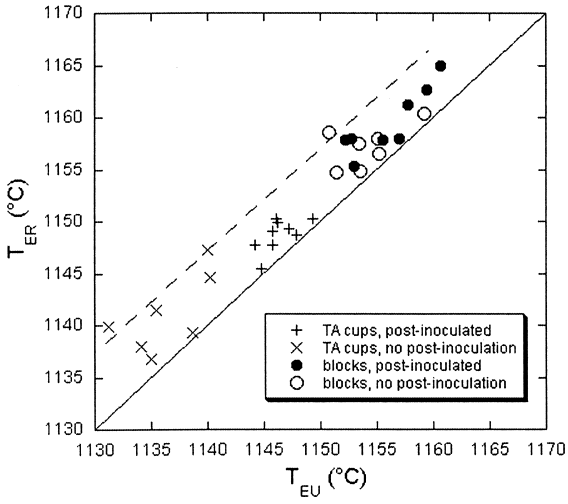

Fig. 2. Plot of the T_{ER} *versus* the T_{EU} values recorded from TA cups and blocks. The distance of the points to the diagonal of the graph (solid line) gives the related recalescence that varies in a band bounded with the interrupted line.

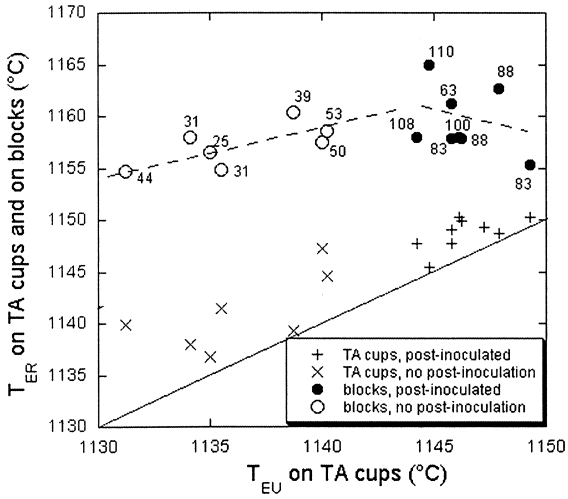

Fig. 3. Plot of the T_{ER} from TA cups and blocks *versus* the corresponding T_{EU} values from TA cups. Numbers are the nodule counts measured on the blocks. The solid line is the same than in Fig. 2 while the interrupted lines are intended to illustrate the apparent trends discussed in the text.

and nodule counts in any of the two clouds of points. This stresses that if there is a relation between the characteristics of the cooling curves and the final solidification microstructure, it does not appear as evident as for small castings. The relation between eutectic solidification in blocks and TA cups, as well as the difference between post-inoculated and no post-inoculated alloys, are somehow summarized in **Fig. 4** where the recalescence ΔT measured on TA cups and the maximum recalescence ΔT_{max} observed on the corresponding blocks have been plotted *versus* the T_{ER} value on TA cups. Recalescence seems to increase with T_{ER} for non post-inoculated melts, for both TA cups and blocks, while it shows apparently no trend for post-inoculated alloys. The use of T_{EU} instead of T_{ER} would have given essentially the same graph though more scattered. Although data scattering may hinder differences between TA cups and blocks, it is interesting to note that such a plot allows differentiating melts according to the use or not of post-inoculation. It is

Table 3. Experimental nodule counts in the centre zone of the blocks (N_{block}), volume fraction (V_V) and area fraction (A_A) affected by CHG.

Code	N_{block} (mm^{-2})	V_V (%)	A_A (%)
M5-4-I	88	9	7
M5-4-N	50	8	1
M5-5-I	86	16	13
M5-5-N	31	1	37
M5-6-I	83	24	20
M5-6-N	31	1	42
M5-10-I	108	16	27
M5-10-I# **	225	12	10
M5-10-N	53	11	7
M5-11-I	100	14	24
M5-11-N	44	7	11
M5-12-I	83	18	47
M5-13-I	63	15	14
M5-13-N	25	0.1	50
M5-16-I	110	22	5
M5-16-N	39	1	50
M5-18-I	88	24	6

** Block chilled in water.

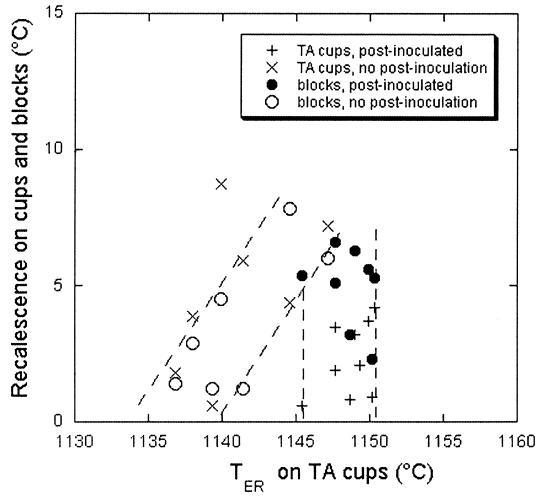

Fig. 4. ΔT on TA cups and ΔT_{max} on blocks *versus* T_{ER} on TA cups. The interrupted lines have been drawn to stress the behaviours mentioned in the text.

however puzzling that recalescence appears similar for TA cups and blocks while it could have been expected to be significantly lower for the blocks because of the higher eutectic plateau temperature and thus the lower driving force for the eutectic transformation. This certainly relates to formation of CHG in blocks and will be discussed later.

In a second step of analysis of the castings, metallographic inspection of the central zones of the blocks was performed. **Figure 5** shows optical micrographs from blocks M5-6-I and M5-11-I in which CHG cells correspond to the areas with fine graphite precipitates, while the remaining of the material consists of the usual microstructure with spheroidal graphite. It was noted that nodules with two different sizes, with diameters respectively from 110 to 160 μm (hereafter called primary nodules) and 30 to 70 μm (hereafter called secondary nodules), were generally observed as in Fig. 5(b). When such two-fold distributions of nodules showed up, the larger ones appeared clearly encapsulated in austenite dendrite-like areas. This two-fold distribution could not however be distinguished when cooling curves presented a strong initial eutectic reaction (associated to T_{EN}) which was the case of trials No. 5 and 6. In these latter blocks, only nodules with 30–70 μm in diameter were found as illustrated in Fig. 5(a). The cooling curves of blocks M5-11-I and M5-6-I, which pertain respectively to the first and second types, are compared in **Fig. 6** where it

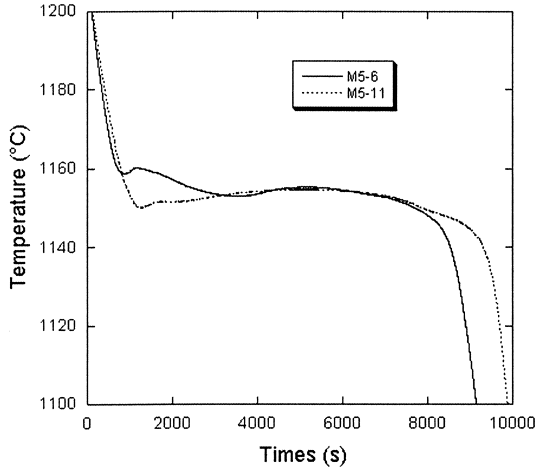

Fig. 6. Cooling curves recorded on post-inoculated M5-6-I and M5-11-I blocks.

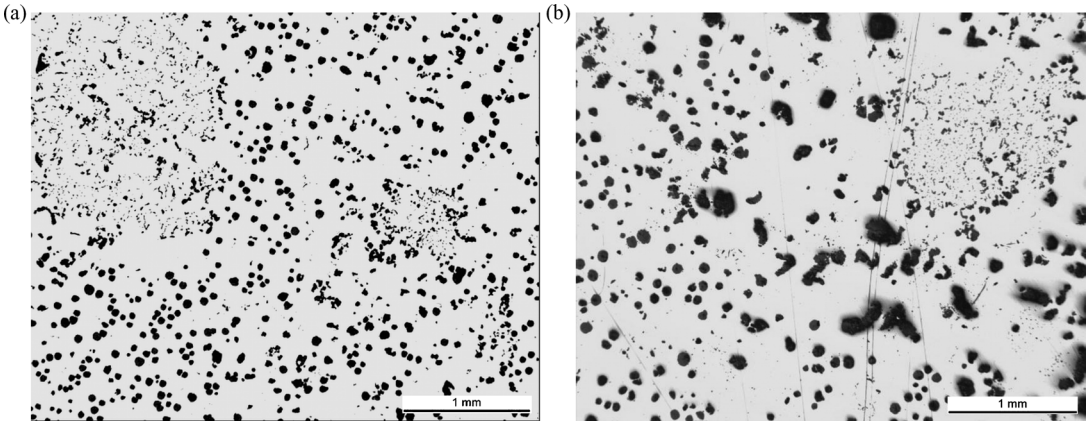

Fig. 5. Micrographs from M5-6-I (a) and M5-11-I (b) blocks. CHG cells correspond to the areas with fine graphite precipitates, while the remaining of the material consists of the usual microstructure with spheroidal graphite.

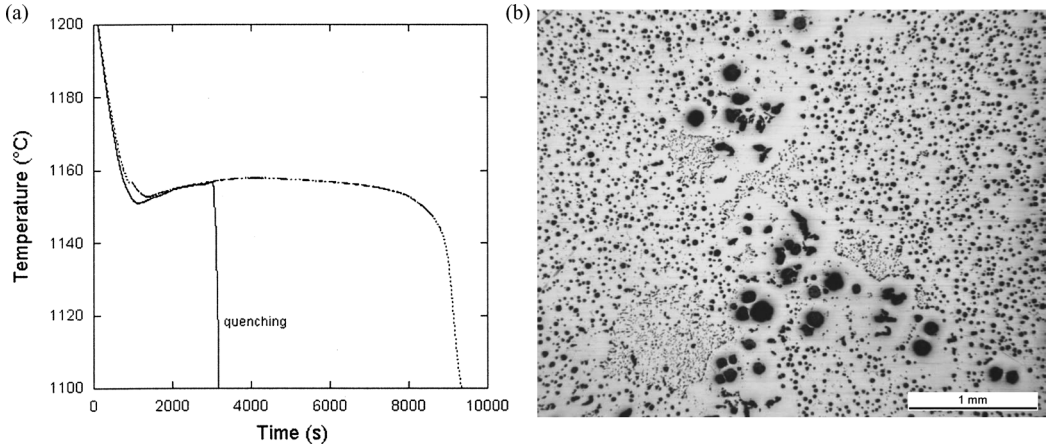

Fig. 7. (a) Cooling curves recorded during trial M5-10 on two blocks of post-inoculated material, one that was let solidify fully and the other one that was quenched; (b) microstructure of the quenched block that shows mostly a matrix with small graphite nodules, but also large nodules embedded in dendrite-like ex-austenite and a few cells of CHG with very fine graphite.

is seen that the T_{EN} arrest proceeds at higher temperature and seems longer for the M5-6-I block than for the M5-10-I one.

The volume fraction V_V of the M5-6-I and M5-11-I blocks affected by CHG were significantly different at 24 and 14% respectively, while the area fraction of CHG in the center, A_A, were quite close at 20 and 24% (see Table 3). Owing to the difference in the V_V value, it was tempting to associate the formation of CHG to the T_{EN} arrest as seen in Fig. 6. However, it appeared impossible to reconcile the results from the whole set of castings with such a hypothesis. In an attempt to withdraw this uncertainty on the time at which CHG cells form, an additional experiment was performed when a block was quenched during solidification (block M5-10-I#). The cooling curve of the quenched block is compared in **Fig. 7**(a) to the one recorded on a block from the same casting that was let cool until complete solidification (M5-10-I). The microstructure of the quenched block is shown in Fig. 7(b) where large nodules embedded in austenite dendrites are seen to have developed to a significant extent. A few CHG cells may be observed aside the dendrites that have a slightly finer structure than those seen on the micrographs in Fig. 5. The remaining of the material has solidified as usual nodular iron, with however a nodule count much higher than the non-quenched block (see Table 3) because of the higher cooling rate achieved during quenching.

This trial strongly suggests that the T_{EN} arrest relates to dendrite-like precipitation of austenite with graphite nodules getting embedded in, CHG cells appearing later. This is in fact much in line with observations made by other authors on smaller samples quenched while undergoing solidification schedule mimicking those of large castings.[42–45] This is also in agreement with previous work[48] where blocks were cast by pairs with and without antimony added, this addition decreasing or even suppressing the formation of CHG as indicated in the introduction. The comparison of the cooling curves from these blocks showed marked differences related to the bulk eutectic solidification (T_{EU} arrest) while the initial eutectic arrests (T_{EN}) were very similar with and without antimony. Growth of CHG cells could thus be related to the bulk eutectic reaction.

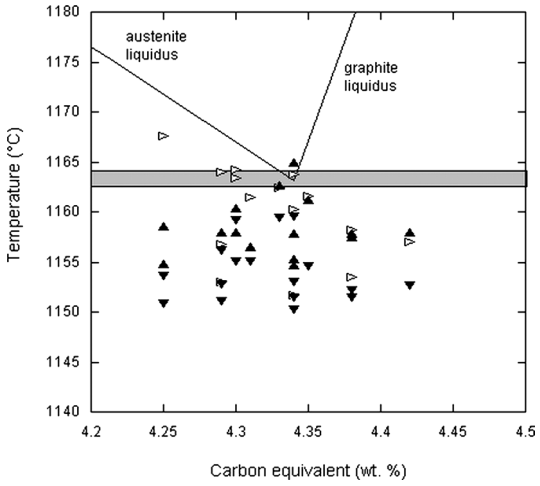

Fig. 8. Plot of the experimental characteristic temperatures from the blocks: upper temperature for the start of solidification, T_L^2 or T_{EN}^2 (horizontal triangles), minimum temperature during solidification, T_{min} (downwards triangles), and maximum temperature during bulk eutectic solidification, T_{ER} (upwards triangles).

4. Discussion

The microstructural features obtained from the present results show some similarities with the schematic proposed by Zhou *et al.*[42] for solidification of spheroidal iron with formation of CHG. These authors proposed a four-step solidification process: 1) nucleation of primary graphite nodules and growth of dendrite-like austenite with graphite nodules getting embedded in; 2) nucleation of CHG cells along the interface of these dendrites with the liquid; 3) growth of the CHG cells; and 4) nucleation of secondary nodules and growth of the corresponding eutectic SG cells. In the following, it is first attempted to compare this schematic with the features obtained from the cooling curves. In a second step, focus will be put on recalescence data in relation to the extent of CHG.

In **Fig. 8** have been plotted as function of the carbon equivalent C_{eq} three of the characteristic temperatures measured on the blocks: i) the upper temperature for the start of solidification, T_L^2 when present or T_{EN}^2 if not (hori-

zontal open triangles), T_{min} (downwards solid triangles) and T_{ER} (upwards solid triangles). The C_{eq} values used for this plot are those given in Table 1, increased by 0.04 wt% for inoculated melts. The graph shows also the stable austenite and graphite liquidus calculated for an average silicon content of 2.2 wt%.[47] The intersection of these two lines gives the stable eutectic temperature for this silicon content, while the greyed area represents the actual range of stable eutectic temperatures reported in Table 1. The large scattering band defined by either of the experimental temperatures T_{min} and T_{ER} appears very similar to the ones shown by Prinz *et al.*[49] who investigated the effect of silicon content of the melt on CHG formation.

Apart for one point at low carbon equivalent, it is seen that all experimental temperatures fall at or below the stable eutectic temperature. Solidification of the blocks thus proceeds from a melt that is undercooled at temperatures at which both austenite and graphite phases could be effectively present. This may not be true for the solidification of the outer skin of the blocks, but it has been shown that the temperature of the material gets homogeneous shortly after pouring of the melt[48] so that this should apply to the most part of each casting. Accordingly, one may thus wonder to which reaction does relate the short T_L arrest that could be sometimes recorded. For answering that question, it seems of interest to stress the size difference between primary and secondary nodules mentioned earlier. If both types of nodules had grown by solid-state diffusion through the austenite shell, the ratio of their sizes could be roughly evaluated using the model proposed by Wetterfall *et al.*[50] According to these authors, the radius R of the graphite nodules at time t writes $R^2-R^2_o \approx \alpha \cdot (t-t_o)$ with R_o the size of the nodules when they get encapsulated by the austenite shell at time t_o, and where α is a temperature dependent coefficient. Considering the nearly isothermal eutectic plateaus in Fig. 6 and setting R_o to zero, the ratio of the radii of the primary to the secondary nodules should then be of the order of $(8\,000/6\,000)^{0.5}$, *i.e.* about 1.15. The fact that this ratio is experimentally much larger leads to conclude that large primary nodules have indeed grown for some time in direct contact with the liquid, possibly giving rise to the short T_L arrest. Though two-fold distribution were generally observed, the presence of the T_L arrest appeared in fact erratic as illustrated with Fig. 7(a) where it shows up on only one of the two curves while both blocks were similarly post-inoculated and cast at the same time with the same melt, and showed similar microstructure.

According to the above description and except for the alloy with the lowest C_{eq} value, growth of austenite proceeds only associated with the T_{EN} arrest, *i.e.* when a sufficient number of graphite nodules have nucleated in the liquid thus allowing for a coupled growth of both phases. In most cases, a significant undercooling with respect to the stable eutectic temperature appeared necessary for this initial eutectic reaction to set up as illustrated with castings M5-11-I in Fig. 6 and M5-10-I in Fig. 7(a). However, very small additional undercooling was needed in the case of blocks M5-5-I and M5-6-I (Fig. 6) and the T_{EN} arrest is at much higher temperature than in the general case. It was not possible to find a clear explanation to this variable undercooling from the present series of experiments, while it could be related to the cerium content of the melt in a parallel investigation.[51] The undercooling of the T_{EN} arrest may be related to carbon supersaturation of the liquid that was suggested by Gagné and Argo[52] to be the main reason for CHG formation. From the present results, it appears however impossible to relate the onset of the T_{EN} arrest with the amount of CHG observed on the blocks, so that other factors than carbon supersaturation should be controlling. One further striking feature of the initial eutectic arrest is that T^1_{EN} appeared similar at given casting conditions (either TA cups or blocks) for a given melt, whenever post-inoculated or not. This is in fact apparent in the graphs of Fig. 1. This would mean that the formation of primary graphite nodules and the set-up of the initial eutectic reaction depend on melt preparation (including pre-inoculation) in the ladle and not on post-inoculation.

According to the above description and in line with the schematic proposed by Zhou *et al.*,[42] CHG cells nucleate after the initial eutectic reaction has proceeded to some extent. When comparing cooling curves of blocks with and without Sb added,[48] it could be observed that the recalescence during the bulk eutectic reaction starting at T_{EU} was much higher in the blocks without Sb. This T_{EU} arrest was however also observed when no (or very few) CHG formed in the blocks with Sb added, in which case it has to relate to nucleation of secondary graphite nodules and growth of the corresponding eutectic cells. As bulk eutectic reaction did always show one single thermal arrest, it should be admitted that nucleation of CHG cells and of secondary nodules are closely related. Thus, in most cases, these two processes should start simultaneously, though one can imagine that either or both of them could as well be continuously spred along the bulk eutectic reaction.

The above observation suggests that eutectic recalescence should increase with the amount of CHG. That CHG growth leads to higher recalescence has been in fact often accepted previously (see the review by Källbom[27]) though very few precise data are available. A close examination of the values reported by Niu and Zhang[43] and Prinz *et al.*[49] do show such a trend although quite scattered. As a matter of fact, only the work by Basutkar and Loper[24] gave enough information about their cooling records for comparison with the present results. The castings studied by these authors were made on different chills, but all presented in their thermal centre cooling curves very similar to those recorded on non-chilled large castings. Thus, excluding data related to the parts of the castings that had been directionally solidified because of the chills, the values of T_{ER} *versus* ΔT_{max} from Basutkar and Loper[24] are plotted in **Fig. 9** with open circles when CHG was observed and solid circles when not. It is seen that CHG is related to the higher eutectic temperatures, but that fully spheroidal graphite structure could be obtained with either lower or higher recalescence. In fact, a closer examination of the data shows that the lowest recalescence values are generally from the thermal centre while the highest values relate to locations away from it. As the melts used in this study have carbon and silicon contents similar to those used by Basutkar and Loper,[24] it seemed meaningful to add the present results in Fig. 9. They are represented with open squares as every block showed some CHG. It is seen that the two sets of re-

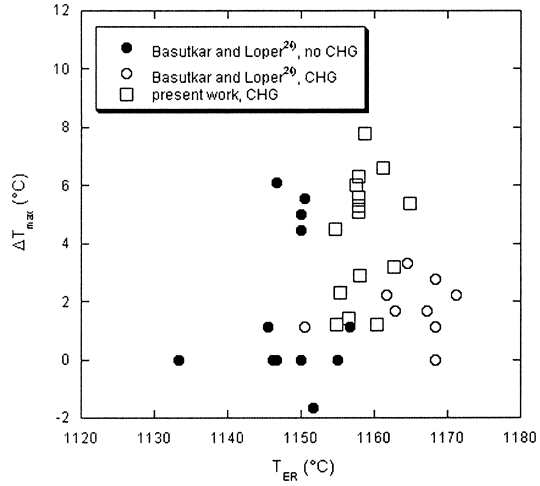

Fig. 9. Correlation between maximum recalescence (ΔT_{max}) and T_{ER} value. Circles are data from Basutkar and Loper,[24] squares from the present work. Open symbols relate to records with CHG, solid symbols without.

sults agree fairly well, though the range of recalescence data recorded in the present work is larger. It has been verified that using T_{EU} instead of T_{ER} would have given a similar graph. This figure shows that CHG leads to eutectic solidification at higher temperature, and this could eventually be associated with a lower carbon supersaturation of the liquid than in the case of solidification without CHG. This would contradict the proposal by Gagné and Argo,[52] though it is recognized that some quantitative information through solidification kinetics modelling would be necessary to ascertain such a conclusion.

In an attempt to go further in the understanding of CHG formation, the possible links between the characteristics of the cooling curves detailed above and the microstructure parameters (V_V and A_A, Table 3) previously presented[46] were looked for. In this previous work, it was noted that V_V increases with the nodule count while the A_A values behave apparently more erratically. It was thus possible to conclude that post-inoculation, which increases nodule count, enhances CHG formation. **Figure 10**(a) shows V_V plotted *versus* the maximum recalescence measured on the blocks. As the points are differentiated according to the fact that they are from melts with or without post-inoculation, the negative effect of post-inoculation is evidenced. A similar graph but surprisingly much more scattered was obtained using ΔT_{EU} in place of ΔT_{max}. It is seen in Fig. 10(a) that recalescence increases first with V_V, up to about 6 to 8°C when V_V is 10 to 15%, and then decreases as more and more of the casting is affected. However, it is worth stressing that the data may be split in two opposite trends, a decrease (resp. increase) of the V_V value with increasing recalescence when post-inoculated (resp. not post-inoculated) melt is used. The main reason for the decrease of recalescence with increased V_V value seems to be thermal exchanges at the scale of the blocks. As a matter of fact, the increase of V_V means that CHG formed earlier in the cooling process of the block, so that a larger volume of remaining melt had to be re-heated leading eventually to lower recalescence. Recalescence may depend also on the undercooling of the melt with respect to the eutectic temperature, but the interplay of these two factors seem to have hindered any possibility to show such correlation from the present results.

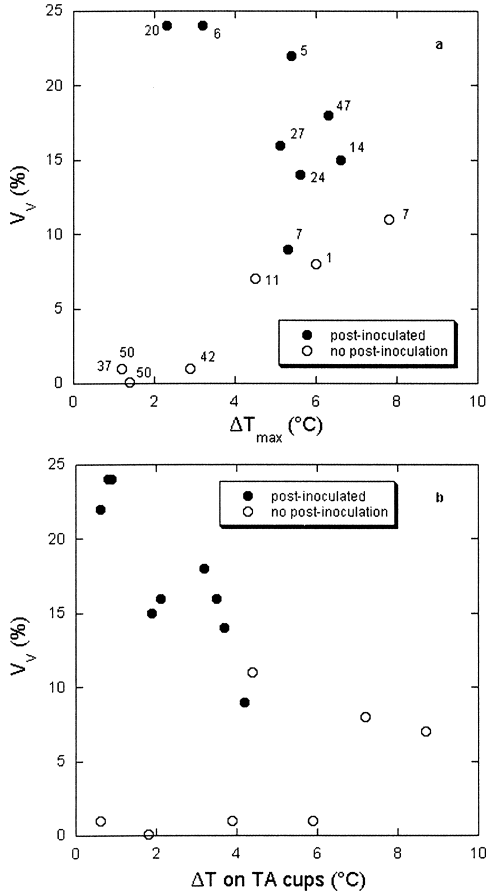

Fig. 10. Plot of V_V *versus* ΔT_{max} measured on blocks (a) and ΔT from TA cups (b). Data aside the points in Fig. 10(a) are the corresponding A_A values.

In Fig. 10(a), the values of A_A have been indicated aside the corresponding points, and it is seen that they appear to change erratically in such a plot, confirming the previous choice of resorting to V_V to characterize the extent of CHG.[46] Interestingly enough, and quite surprisingly, plotting V_V against ΔT from cups leads to the plot shown in Fig. 10(b) that shows similar features than Fig. 10(a), with a decrease of V_V with an increase of ΔT up to a maximum value, then a parallel decrease of both quantities at very low V_V values. Such a relation, if confirmed, could be useful for quality control of post-inoculated melts before casting but would need to be fully understood. It has been verified that the relation shown is not due to the nodule count, and this calls for further experiments for a better understanding.

5. Conclusion

Thermal analysis of large blocks cast with spheroidal graphite cast irons prone to give chunky graphite showed up to three distinct thermal arrests, all at temperatures lower than the stable eutectic temperature. This is true for all near-eutectic melts used in the present study, either hypo-eutectic or hyper-eutectic with carbon equivalent ranging from 4.28 to 4.38 (or even 4.42 if post-inoculation is accounted for). Comparison of the cooling curves characteristics with microstructure evaluation gives the following

solidification sequence: 1) nucleation of primary graphite in the liquid (T_L arrest that is not always recorded); 2) initial eutectic reaction processing by growth of austenite-like dendrites encapsulating the primary nodules (T_{EN} arrest); 3) bulk eutectic reaction related to nucleation and then growth of CHG cells and of secondary nodules, these latter giving spheroidal graphite eutectic cells (T_{EU} arrest). The onset temperature of the initial eutectic reaction appeared to depend strongly on initial melt preparation and not on the use of in-mould post-inoculation. The thermal arrest at the start of the bulk eutectic reaction was more or less marked depending on the final recalescence undergone during the transformation. By plotting the volume of the blocks affected by chunky graphite as function of recalescence, it was found that the maximum recalescence during the eutectic reaction first increases with the volume of the block affected by CHG, and then decreases when most of the material is affected. While the increase may be understood because of the high growth rate of the CHG cells, the decrease may relate to thermal exchanges at the scale of the blocks. Surprisingly enough, it has been found a relationship between the volume of the blocks affected by CHG and the recalescence observed on TA cups. Such a relationship, that could be of great help for melt preparation, should be further investigated.

Acknowledgements

This paper is based on work supported by the Industry Department of the Spanish Government (PROFIT FIT-030000-2007-94).

REFERENCES

1) M. D. Chaudhari, R. W. Heine and C. R. Loper: *AFS Trans.*, **82** (1974), 379.
2) M. F. Basdogan, V. Kondic and G. H. Bennett: *AFS Trans.*, **90** (1982), 263.
3) D. M. Stefanescu, C. R. Loper, Jr., R. C. Voigt and I. G. Chen: *AFS Trans.*, **90** (1982), 333.
4) I.-G. Chen and D. M. Stefanescu: *AFS Trans.*, **92** (1984), 947.
5) P. Zhu and R. W. Smith: *AFS Trans.*, **103** (1995), 601.
6) C. Labrecque and M. Gagné: *AFS Trans.*, **106** (1998), 83.
7) G. R. Strong: *AFS Trans.*, **91** (1983), 151.
8) J. M. Frost and D. M. Stefanescu: *AFS Trans.*, **100** (1992), 189.
9) P. Larrañaga, J. Sertucha and R. Suárez: *Rev. Metal. Madrid*, **42** (2006), 244.
10) J. Sertucha, R. Suárez, J. Izaga, L. A. Hurtado and J. Legazpi: *Int. J. Cast Met. Res.*, **19** (2006), 315.
11) U. Ekpoom and R. W. Heine: *AFS Trans.*, **89** (1981), 27.
12) J. O. Barlow and D. M. Stefanescu: *AFS Trans.*, **105** (1997), 349.
13) J. Tinoco, P. Delvasto, O. Quintero and H. Fredriksson: *Int. J. Cast Met. Res.*, **16** (2003), 53.
14) J. F. Wallace: *AFS Trans.*, **83** (1975), 363.
15) R. Monroe and C. E. Bates: *AFS Trans.*, **90** (1982), 307.
16) C. A. S. Ribeiro, D Santos, W. Baumgart, F. Vilela and C. Henke: *Int. J. Cast Met. Res.*, **16** (2003), 47.
17) R. Doepp and S. Schwenkel: *Mater. Sci. Eng.*, **A413–414** (2005), 338.
18) A. Suárez-Sanabria and J. Fernández-Carrasquilla: *Rev. Met. Madrid*, **42** (2006), 18.
19) S. Chang, D. Shangguan and D. M. Stefanescu: *AFS Trans.*, **99** (1991), 531.
20) A. Louvo, E. Pellikka, J. Alhainen and P. Eklund: *AFS Trans.*, **99** (1991), 237.
21) F. J. Bradley and C. A. Fung: *Can. Metall. Q.*, **30** (1991), 251.
22) P. Larrañaga, J. M. Gutiérrez, A. Loizaga, J. Sertucha and R. Suárez: *AFS Trans.*, **116** (2008), 547.
23) P. K. Basutkar and C. R. Loper: *AFS Trans.*, **79** (1971), 169.
24) P. K. Basutkar and C. R. Loper: *AFS Trans.*, **79** (1971), 176.
25) Z. Ignaszak: *Int. J. Cast Met. Res.*, **16** (2003), 93.
26) R. Källbom, K. Hamberg, M. Wessén and L. E. Björkegren: *Mater. Sci. Eng.*, **A413–414** (2005), 346.
27) R. Källbom, K. Hamberg and L. E. Björkegren: Proc. of Gjutdesign 2005 final seminar, VTT Technical Resarch Centre of Finland, Espoo, (2005), 1.
28) S. I. Karsay and E. Campomanes: *AFS Trans.*, **78** (1970), 85.
29) R. Barton: BCIRA report 1436, (1981), 340.
30) H. Itofuji and H. Uchikawa: *AFS Trans.*, **98** (1990), 429.
31) B. C. Liu, T. X. Li, Z. J. Rue, X. Y. Yang, E. Q. Huo and C. R. Loper: *AFS Trans.*, **98** (1990), 753.
32) A. Javaid and C. R. Loper: *AFS Trans.*, **103** (1995), 135.
33) E. N. Pan, C. N. Lin and H. S. Chiou: *AFS Trans.*, **103** (1995), 265.
34) M. Wessén, I. L. Svensson and R. Aagaard: *Int. J. Cast Met. Res.*, **16** (2003), 119.
35) R. Källbom, K. Hamberg and L. E. Björkegren: Proc. 67th World Foundry Cong., Harrogate, UK, (2006), paper 184.
36) E. Campomanes: *Giesserei*, **65** (1978), 535.
37) T. C. Xi, J. Fargues, M. Hecht and J. C. Margerie: *Mat. Res. Soc. Symp. Proc.*, **34** (1985), 67.
38) R. K. Buhr: *AFS Trans.*, **76** (1968), 497.
39) P. K. Basutkar., C. R. Loper and C. L. Babu: *AFS Trans.*, **78** (1970), 429.
40) C. R. Loper, R. W. Heine, R. W. Reesman and B. H. Shah: *AFS Trans.*, **75** (1967), 75, 547.
41) Z. Li and Y. Li: *Metall. Mater. Trans. A*, **36A** (2005), 2455.
42) J. Zhou, W. Schmitz and S. Engler: *Giesserei-Forschung*, **39** (1987), 55.
43) Y. Niu and Z. Zhang: *The Foundryman*, **81** (1988), 390.
44) Z. Zhang, H. M. Flower and Y. Niu: *Mater. Sci. Technol.*, **5** (1989), 657.
45) H. Itofuji and A. Masutani: *Int. J. Cast Met. Res.*, **14** (2001), 1.
46) I. Asenjo, P. Larrañaga, J. Sertucha, R. Suárez, I. Ferrer, J. M. Gómez and J. Lacaze: *Int. J. Cast Met. Res.*, **20** (2007), 319.
47) M. Castro, M. Herrera, M. M. Cisneros, G. Lesoult and J. Lacaze: *Int. J. Cast Met. Res.*, **11** (1999), 369.
48) P. Larrañaga, I. Asenjo, J. Sertucha, R. Suárez, I. Ferrer and J. Lacaze: to appear in *Int. J. Cast Met. Res.*
49) B. Prinz, J. Reifferscheid, T. Schulze, R. Döpp and E. Schürmann: *Giessereiforschung*, **43** (1991), 107.
50) S.-E. Wetterfall, H. Fredriksson and M. Hillert: JISI, May 1972, 323.
51) P. Larrañaga, I. Asenjo, J. Sertucha, R. Suárez, I. Ferrer and J. Lacaze: *Metall. Mater. Trans. A*. DOI: 10.1007/s11661-008-9731-y.
52) M. Gagné and D. Argo: Proc. Int. Conf. of Advanced Casting Technology, Part I and II, ed. by J. Easwaren, ASM Int., OH, (1987), 231.